Broad-Band Small-Signal Impedance Characterization of Silicon (Si) P^+-N-N^+ IMPATT Diodes

MOTOHARU OHTOMO

Abstract—A method is described that permits a broad-band small-signal characterization of an IMPATT diode mounted in a package. From automatic-network-analyzer measurements on a package-shaped metal dummy, an empty package, and the diode under test biased below and above breakdown, the method allows first determination of a coupling-circuit parameter, bonding-wire inductance, and diode series resistance, and then evaluation of junction admittance above breakdown.

Experimental results on silicon (Si) p^+-n-n^+ diodes over 2.5–15 GHz are shown. Nearly frequency-independent bonding-wire inductance is observed. Avalanche frequency squared (f_a^2) is found to be sublinear with respect to dc current density (I_d), possibly due to a variation of junction temperature (T_j). An experimental formula for f_a^2/I_d is obtained in terms of T_j. Detailed comparisons of the measured junction admittance with an existing analytical theory indicate a good agreement, if a suitable amount of saturation current is postulated, and also suggest that the estimated amount is in excess of the prebreakdown saturation current.

I. INTRODUCTION

MICROWAVE impedance measurements of IMPATT diodes are important both for evaluating the diode capability, and for designing optimum circuits. In order to fulfill these purposes, not only small-signal measurements [1], [2] but also large-signal ones [3]–[6] are required. Nevertheless, the former are still useful in investigating the fundamental diode parameters and in examining the diode quality by comparison with analytical theories [7], [8] or computer simulations [9].

For accurate evaluation of the active diode impedance, the parameters of a coupling circuit between a measurement reference plane and the diode port must be calibrated beforehand with adequate known impedances. For instance, Dunn and Dalley [1] evaluated the bonding-wire inductance, diode series resistance, and active impedance after determining the impedance matrix outside the diode package, by use of a package-shaped metal dummy, an empty package, and a ceramic disk. Meanwhile, Gewartowski and Morris [3], and Steinbrecher and Peterson [2] employed variable junction capacitance of the diode under test with series resistance variation calculated [3] or neglected [2], for determining the circuit parameters outside the active region. So far as the active impedance is concerned, the method in [3] or [2] seems to be more accurate, since impedance measurements on only the diode under test are enough and junction capacitance can usually be considered frequency independent up to microwave frequencies of interest. Such a method, however, is incapable of determining the series resistance that has detrimental effects on diode efficiency [10], unless the circuit loss is evaluated otherwise. In practical applications, the value of bonding-wire inductance also becomes necessary for considering the transformation of diode impedance within a package. The method in [1] seems attractive in these respects.

This paper presents an alternative method which permits broad-band junction-admittance measurements of an IMPATT diode as well as its series resistance and bonding-wire inductance. As a means of calibration, the method utilizes a metal dummy of a package shape, an empty package, and variable junction capacitance of the diode under test, which are partly common with those in [1]–[3]. Here, however, an introduction of a unique measurement reference plane and data reduction technique makes it unnecessary to know the value of the empty package capacitance. Furthermore, use of variable junction capacitance will enable one to obtain an accuracy in the active admittance of the same degree as in [3] or [2] without the need of calculation or neglect of series-resistance variation. A technique of compensating for a small circuit is also presented. Then the small-signal results obtained over 2.5–15 GHz are illustrated on X-band silicon (Si) p^+-n-n^+ IMPATT diodes. The measured active admittance is compared with that obtained by similar methods, as in [3] and [2]. Finally, the measured admittance is compared in detail with an analytical theory by Hulin *et al.* [8] with special emphasis on the saturation-current effect. An observed sublinearity in avalanche frequency squared against dc bias current is also discussed with respect to junction-temperature variation.

II. MEASUREMENT METHOD

A. Measurement Setup

Impedance measurements were performed with an automatic network analyzer (Hewlett-Packard, model 8540) over a frequency range of from 2.5 to 15 GHz at a signal level ≈ -20 dBm to ensure a small-signal condition. Fig. 1 shows the 50-Ω coaxial test mount and the diode package used. The dc bias was fed from the left of the mount through a biasing network, which, however, was included as a part of the analyzer during its calibration

Manuscript received October 16, 1973; revised February 11, 1974.
The author is with the Toshiba Research and Development Center, Tokyo Shibaura Electric Company, Ltd., Kawasaki, Japan.

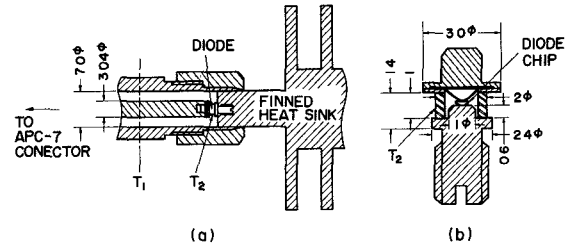

Fig. 1. (a) 50-Ω coaxial test mount. (b) Package dimensions in millimeters.

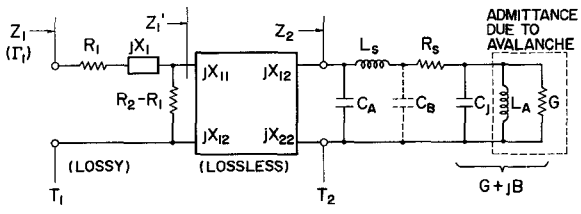

Fig. 2. Equivalent circuit of test mount.

procedures. No diode oscillation occurred with this configuration over the whole bias range. The equivalent circuit of the mount is represented by Fig. 2 [11], [1], where T_1 and T_2 are the reference planes chosen in the coaxial line and at the outer surface of the package ceramics, respectively, as shown in Fig. 1. The coupling circuit between T_1 and T_2 can generally be decomposed into a lossy and lossless circuit [12]. Elements to the right of T_2 represent package capacitance C_A ($=0.20$ pF at 1 MHz), bonding-wire inductance L_s,[1] fringing capacitance C_B, series resistance R_s,[1] and junction capacitance C_j. G and L_A represent the additional conductance and inductance, respectively, due to avalanche [9]. C_A, L_s, R_s, G, and L_A may not necessarily be frequency independent. C_B is very small, typically $\lesssim 0.05$ pF as estimated from the diode chip geometry. Since $\omega C_B R_s \ll 1$ holds even at the microwave frequencies of interest, C_B was included in C_j as at lower frequencies by transferring it to the right of R_s.

B. Principle of the Method—Lossless Case

If the coupling circuit is lossless, i.e., $R_1 = 0$ and $R_2 = \infty$ in Fig. 2, the position of T_1 can be chosen such that $X_{22} = 0$, giving

$$Z_1 = jX_{11} + X_{12}^2/Z_2 \tag{1}$$

where Z_1 and Z_2 are the impedances seen to the right of T_1 and T_2, respectively, and jX_1 is included here in jX_{11}. In other words, at such T_1, Z_1 becomes infinite or reflection coefficient Γ_1 is equal to 1 for $Z_2 = 0$. Employing a package-shaped metal dummy as a short ($Z_2 = 0$), the position of T_1 can easily be determined.

[1] The diode-mounting stud also contributes to L_s. The contribution, however, was estimated to be small, ≈ 0.06 nH, with an inductance formula in [13]. R_s also includes $\lesssim 0.1$-Ω skin resistance [13] of the four parallel-connected gold bonding wires with 25-μm diameter and ≈ 1-mm length.

Let Z_{1p} and $Z_1(V)$ be the measured values of Z_1 for an empty package and the diode biased at dc reverse voltage V, respectively. Then we have, from (1),

$$Z_{1p} = jX_{11} + X_{12}^2 \cdot j\omega C_{AE} \tag{2}$$

$$Z_1(V) = jX_{11} + X_{12}^2 \cdot \left[j\omega C_A + \frac{1}{R_s(V) + j\omega L_s + 1/\{G(V) + jB(V)\}} \right] \tag{3}$$

where C_{AE} is the empty package capacitance. If we can assume $C_{AE} = C_A$, we have, from (2) and (3),

$$1/[Z_1(V) - Z_{1p}] = [R_s(V) + j\omega L_s + 1/\{G(V) + jB(V)\}]/X_{12}^2. \tag{4}$$

Especially for $V \leq V_{br}$ (breakdown voltage), (4) can be decomposed into

$$\text{Re}\,\{1/[Z_1(V) - Z_{1p}]\} = R_s(V)/X_{12}^2 \tag{5}$$

$$\text{Im}\,\{1/[Z_1(V) - Z_{1p}]\} = [\omega L_s - 1/\omega C_j(V)]/X_{12}^2 \tag{6}$$

since $G(V) + jB(V) = j\omega C_j(V)$. Equation (6) implies that, at a fixed frequency, the plots of Im $\{1/[Z_1(V) - Z_{1p}]\}$ versus $1/\omega C_j(V)$ for various values of V should be on a straight line whose slope and interaction with the vertical axis are $-1/X_{12}^2$ and $\omega L_s/X_{12}^2$, respectively. If C_j measured at a low frequency (e.g., 1 MHz) is employed, X_{12}^2 and L_s can be determined. $R_s(V)$ can then be evaluated from (5). Above breakdown, it is possible to evaluate $R_s(V) + 1/\{G(V) + jB(V)\}$ from (4). If $R_s(V) = R_s(V_{br})$ is postulated as in [1]–[3], we have $G(V) + jB(V)$. Note here that the value of C_A or C_{AE} at the microwave frequency is not required in the preceding procedures.

Various assumptions made either explicitly or implicitly so far will be examined. For a coupling circuit with a small loss, the present method still applies after minor modifications, as shown later. The equivalent circuit of a packaged diode shown in Fig. 2 has been frequently used and its validity has been directly confirmed, for instance, in [6] for a package that has a diode-mounting stud of a height lower than that of the ceramics. The latter condition is apparently satisfied by the present package. The frequency independence of the junction capacitance up to microwave frequencies is well established in IMPATT diodes [3], [6]. The package dimensions in Fig. 1(b) evidently conform to Getsinger's criterion for a package to couple the coaxial line via a radial line of the dominant E-type mode [11]. Moreover, the package height ($=1.4$ mm) is sufficiently less than the spacing ($=2.5$ mm) between T_2 and the outer conductor of the coaxial line. Hence, the field configurations associated with the metal dummy will still be similar enough for the dummy to be regarded as a short of the radial line. Generally, $R_s(V)$ is not constant above breakdown, and the true values of G and B, denoted here by G_t and B_t, respectively, are given by

$$G_t = G + \Delta R_s(G^2 - B^2) \tag{7}$$

$$B_t = B + 2\Delta R_s GB \tag{8}$$

for $\Delta R_s G$ and $\Delta R_s B \ll 1$, where $\Delta R_s \equiv R_s(V) - R_s(V_{br})$. These corrections are, however, expected to be small, as illustrated later in Section III-B.

Package capacitance C_A has a small variation ($\approx \pm 0.005$ pF) between different packages. By denoting $\Delta C \equiv C_A - C_{AE}$ and retaining the terms to the first order of $\Delta C/C_A$ in (2) and (3), we have equations identical to (5) and (6) except that X_{12}^2, L_s, $R_s(V)$, and $C_j(V)$ are replaced by the following primed quantities:

$$X_{12}'^2 = X_{12}^2(1 - 2\omega^2 L_s \Delta C) \qquad L_s' = L_s(1 - \omega^2 L_s \Delta C)$$

$$R_s'(V) = R_s(V)[1 + 2\omega\Delta C\{\omega L_s - 1/\omega C_j(V)\}]$$

$$C_j' = C_j + \Delta C.$$

The junction capacitance measured at 1 MHz is just this $C_j'(V)$, which is evaluated as the difference between the capacitances of the diode under test and the reference empty package. Thus the previously described procedures to evaluate X_{12}^2, L_s, and $R_s(V)$ actually give the primed quantities. The differences between them are, however, usually expected to be small. For example, we have $|(L_s' - L_s)/L_s| \approx 0.012$ and $|\{R_s'(V) - R_s(V)\}/R_s(V)| \approx 0.008$ at 10 GHz for $\Delta C = 0.01$ pF, $L_s = 0.3$ nH, and $C_j'(V_{br}) = 0.7$ pF. In fact, within the spreads of the measurements, no dependence of L_s on ω^2 was observed (see Fig. 5), except when an empty package with unusually large C_{AE} was employed intentionally.

C. Circuit-Loss Compensation

The reflection coefficients $|\Gamma_1|$ for the metal dummy and empty package in the actual circuit were found to lie between 0.98 and 1, indicating the presence of a small loss in the coupling circuit.[2] A technique of removing the circuit-loss effect is described below. In the coupling circuit shown in Fig. 2, $R_1 + jX_1$ and $R_2 + jX_2$ correspond to the points with minimum and maximum real parts, respectively, on an impedance circle C, which is the locus of Z_1 for pure reactance Z_2 varying from $-j\infty$ to $j\infty$ [12]. Let us choose again the position of T_1 such that $\angle \Gamma_1 = 0°$ for $Z_2 = 0$, and denote Z_1's for the metal dummy and empty package by R_m and $R_p + jX_p (= Z_{1p})$, respectively. For example, $R_m = 4950\ \Omega$ and $R_p + jX_p = 0.38 + j30.5\ \Omega$ at 10.5 GHz, at which R_m was smallest among the measured. Since circle C should contain R_m and $R_p + jX_p$, and also should lie on the right-half plane, R_1 and R_2 are restricted as follows:

$$0 \le R_1 \le R_p \quad (= 0.38\ \Omega)$$

$$0 \le R_2 - R_m \lesssim R_p + |X_p|[|X_p| + 2(R_m R_p)^{1/2}]/R_m \quad (= 1\ \Omega)$$

where $|R_p/R_m| \ll 1$ and $|X_p/R_m| \ll 1$ are taken into account. Throughout this section, every numerical example shown in parentheses is for 10.5 GHz. Thus we have $R_1 \lesssim 1\ \Omega$ and $R_2 \doteqdot R_m \gg 1$ with little error. It can be shown further that

$$|X_{22}| \doteqdot (X_{12}^2/R_m)[(R_2 - R_m)/R_m]^{1/2} \ll 1 \quad (\lesssim 0.008\ \Omega)$$

and

$$X_1/(R_2 - R_1) \doteqdot [(R_2 - R_m)/R_m]^{1/2} \ll 1 \quad (\lesssim 1/70)$$

where a knowledge of $X_{12}^2 \approx 3000\ \Omega^2$ and $|X_{11} + X_1| \doteqdot |X_p - X_{12}^2 \omega C_{AE}| \ll R_m[R_m/(R_2 - R_m)]^{1/2}$, obtained under the lossless assumption, is utilized. Hence, we are allowed to take $X_{22} = 0$ without significant error in the present case; or we can apply the same data reduction technique as in the lossless case, if we use $Z_1'(V)$ and Z_{1p}' instead of $Z_1(V)$ and Z_{1p}, respectively, in Fig. 2. Actually, however, an approximate circuit in Fig. 3 was used due to an indefiniteness in jX_1. This is equivalent to bringing the center of circle C onto the real axis, or to taking $R_2 = R_m$, $X_1 = 0$, and $R_1 = R_p - X_p^2/(R_m - R_p)$ in Fig. 2. $Z_1''(V)$ and Z_{1p}'' can then be evaluated and used instead of $Z_1'(V)$ and Z_{1p}', respectively. The possible absolute error in the left-hand side of (4) caused by this approximation can be estimated to be less than $3|X_1|/R_m^2$ ($\lesssim 9 \times 10^{-6}$ mho) for $|Z_1''(V)| \gtrsim R_m$. For $|Z_1''(V)| \lesssim R_m$, the relative error will be less than $3|X_1|/R_m$ ($\lesssim 0.04$).

This technique of compensating for the circuit loss has been found to reduec R_s by $\lesssim 0.5\ \Omega$ from the uncompensated value and its spreads between frequencies, with essentially no change in reactive quantities such as X_{12}^2 and L_s. Note that active admittance $G + jB$ might be evaluated fairly accurately without this compensation technique, since the circuit loss then incorporated in R_s would be partly cancelled in obtaining $G + jB$ from (4). In Section III, $Z_1''(V)$ and Z_{1p}'' are quoted without double primes.

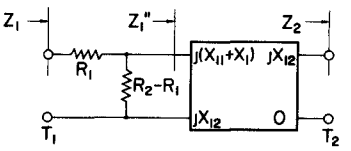

Fig. 3. Approximate circuit used for compensating for a small loss in coupling circuit in Fig. 2.

III. EXPERIMENTAL RESULTS

The diodes investigated are X-band Si p^+-n-n^+ IMPATTs (Toshiba S3019) which have a nearly abrupt junction with depth $x_j \approx 2\ \mu$m and surface impurity concentration $N_s \approx 1 \times 10^{20}$ cm^{-3}. Other parameters are summarized in Table I. Impedance measurements were performed with the automatic network analyzer on a package-shaped metal dummy, an empty package, and the diode under test biased into various reverse voltages below and above breakdown. The data printed out by the analyzer were reduced with another electronic computer to evaluate the following parameters.

[2] If the circuit is lossless, both the gold-plated dummy and the empty package with alumina ceramics ($\tan\delta \approx 1 \times 10^{-3}$) will give $|\Gamma_1| \gtrsim 0.999$ at 10 GHz.

TABLE I
VARIOUS PARAMETERS OF THE Si IMPATT DIODES INVESTIGATED

	Diode #1	Diode #2
Breakdown voltage, V_{br} (volt)	63	70
Junction capacitance at V_{br}, C_{jb} (pF) (measured at 1 MHz)	0.66_1	$0\ 72_7$
Junction area, A (10^{-4} cm^2)	2.0_1	2.3_8
Depletion layer length at V_{br} (μm)	3.1_8	3.4_2
Thermal resistance (°C/W)	16.5	19.0
Oscillation power output at 11 GHz (mW)	418	625
Bias current (mA)	98	119
Efficiency (%)	5.8	6.3
Bonding-wire inductance, L_s (nH) (averaged over 2.5 - 15 GHz)	0.335 ± 0.01	0.274 ± 0.004
Series resistance at V_{br} (ohm) (averaged over 8 - 12 GHz)	0.67 ± 0.1	0.53 ± 0.09

A. Determination of X_{12}^2, L_s, and R_s

At reference plane T_1, $\angle \Gamma_1$ of the empty package was found to lie between 167.9° and 95.2° for frequencies from 2.5 and 15 GHz. With an increase of bias voltage from 1 V to V_{br}, Γ_1 for diode number 2, for example, varied continuously from $0.929 \angle 27.0°$ to $0.990 \angle 108.4°$ at 2.5 GHz, and from $0.933 \angle -53.0°$ to $0.979 \angle -22.6°$ at 15 GHz.

Fig. 4 shows an example of imaginary and real part of $1/[Z_1(V) - Z_{1p}]$ versus $1/\omega C_j(V)$ at 10 GHz. The plots of Im $\{1/[Z_1(V) - Z_{1p}]\}$ versus $1/\omega C_j(V)$ are seen to lie very closely on a straight line as expected. In the computer data reduction, X_{12}^2 and L_s were evaluated from the line determined by a least squares method. The standard deviation (sigma) of the data from the line was found to be very small, typically below 0.02 mmho for each frequency of measurement. Therefore, in order to save measurement time, it seems possible to reduce the number of $Z_1(V)$ measurements without significant loss of accuracy. X_{12}^2 was found to be a nearly monotonically increasing function of frequency, varying from 2600 to 3340 Ω^2 for 2.5–15 GHz. Meanwhile, L_s is seen to be nearly frequency independent within the spreads of the measurement as shown in Fig. 5. Its sigma is only 1.5 percent of the average value $\bar{L}_s$.

The average and sigma of the series resistance R_s over 8–12 GHz (0.5-GHz step) are shown in Fig. 6 as a function of $1/C_j$, which is proportional to the depletion layer length. Owing to the fact that R_s is usually an order of magnitude smaller than $\omega L_s - 1/\omega C_j$, its sigma is relatively large and $\approx 0.2\ \Omega$ at maximum. The accuracy of R_s measured with the present method will be mainly limited by the measurement error in $|\Gamma_1|$, which is nominally within ± 0.01 for $|\Gamma_1| \approx 1$ [14]. The error is equivalent to ± 0.3-Ω uncertainty in R_s as estimated by using (4). Due to some randomness in this type of error, the averaged R_s seems to have less uncertainty. The electrical repeatability of the coaxial test mount also affects R_s. It was, however, felt good, since 1 h later remeasurement on the metal dummy resulted in differences of 0.003 in $|\Gamma_1|$ and 0.4° in $\angle \Gamma_1$ on a root-mean-square basis.

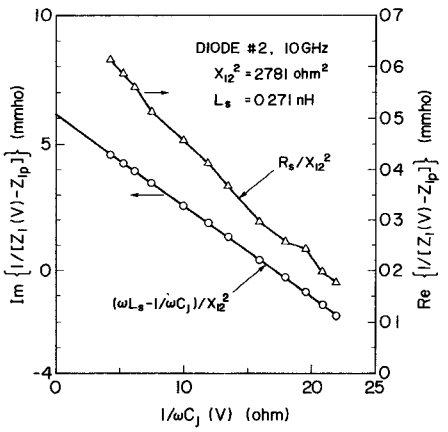

Fig. 4. Real and imaginary parts of $1/[Z_1(V) - Z_{1p}]$ versus $1/\omega C_j(V)$ at 10 GHz.

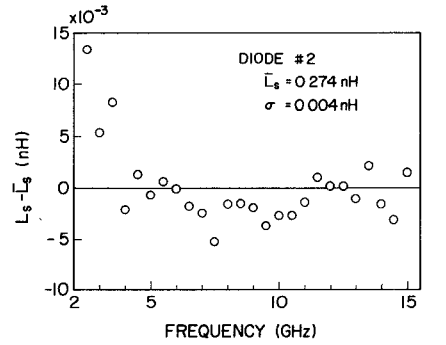

Fig. 5. Deviation of measured bonding-wire inductance L_s around its average value $\bar{L}_s$.

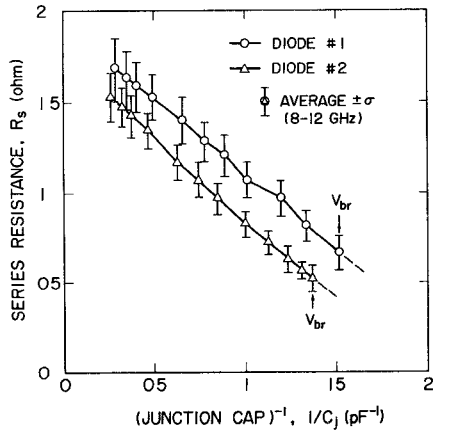

Fig. 6. Measured series resistance versus $1/C_j$ below breakdown.

Since the depletion region widens mainly towards the n layer at higher reverse voltage, the slope of the curves for $1/C_j \gtrsim 1$ pF^{-1} in Fig. 6 approximately equals $-\epsilon\rho$, where ϵ is the dielectric constant ($=1.045$ pF/cm for Si) and ρ the resistivity of the n layer at an edge of the depletion region. Especially, diode number 2 is seen to have a uniform $\rho \approx 0.76\ \Omega \cdot$cm.

B. Junction Admittance Above Breakdown

Diode impedance above breakdown has been measured for 12 different bias conditions. The small-signal junction admittance $G + jB$ was evaluated from (4), assuming $R_s(V) = R_s(V_{br})$. RF voltage across the junction was estimated to be less than 0.05 V for a measurement power level of -20 dBm. The results are illustrated in Fig. 7.[3] They exhibit, at least qualitatively, most of the salient features of an IMPATT as demonstrated by Misawa's computer simulation [9]. Contrary to the simulation, however, one can readily see $f_B < f_G$, where f_B and f_G are the characteristic frequencies at which B and G change their signs, respectively.

If $\Delta C(= C_A - C_{AE})$ and C_B, which was included in C_j, are not zero, measured $G + jB$ will have a small offset $\approx -2\omega\Delta C(\omega L_s G) + j\omega\Delta C(1 - 2\omega L_s B) + j\omega C_B$ from the true value for $\omega L_s \mid G + jB \mid \ll 1$. This will then cause f_B to have an offset $\Delta f_B \doteqdot -f_B(C_B + \Delta C)/(\partial B/\partial\omega)_{f_B}$, where $(\partial B/\partial\omega)_{f_B} = 1.2 \sim 1.4$ pF ($\approx 2C_{jb}$) as seen from Fig. 7. Since C_B ($\lesssim 0.05$ pF) is usually considered larger than $\mid \Delta C \mid$ ($\lesssim 0.005$ pF), f_B is likely to be measured $\lesssim 4$ percent lower than the true f_B intrinsic to the junction. Nevertheless, this still seems insufficient to explain the observed $f_B < f_G$, especially for diode number 2.

In order to examine the accuracy of the measurement method, comparison was made between $G + jB$ measured with the present and other methods (GM and SP). Methods GM and SP correspond to those presented in [3] and [2], respectively, except the numerical procedures. In both methods, the coupling-circuit parameters outside the active region were determined from the measured reflection coefficients for ≥ 3 values (e.g., 12 values) of $R_s(V) - j/\omega C_j(V)$ below breakdown, by employing a least squares technique [15] which was modified from Kajfez's procedure [16]. For method GM, $R_s(V) - R_s(V_{br})$ obtained from Fig. 6 was employed instead of $R_s(V)$; for method SP, $R_s(V)$ was assumed to be 0. A typical comparison of $G + jB$ is illustrated in Fig. 8, where a good agreement can generally be found. Fractional differences in f_B and f_G between the present method and methods GM or SP have been found to be $0.003 < \delta f_B/f_B \lesssim 0.02$ and $-0.005 \lesssim \delta f_G/f_G \lesssim 0.015$ almost independently of bias conditions for both diodes, indicating that the relationship $f_B < f_G$ observed in Fig. 7 is left unaltered. It should be remarked that method SP, or neglect of R_s variation, almost always gave $\mid G \mid$ about 10 percent smaller than method GM when $G < 0$, while both methods gave essentially no difference in B.

The assumption of $R_s(V) = R_s(V_{br})$ is next examined. Above breakdown, junction temperature T_j and V increase with dc input power. Accordingly, the depletion layer widens in a nonpunched-through diode, resulting in a decrease of R_s. Meanwhile, resistivity of Si outside the depletion region usually increases with T_j, roughly by a

[3] Data at 14.5 GHz are omitted, since jB was found more than 10-percent output of values, as expected from data at neighboring frequencies, possibly due to some errors.

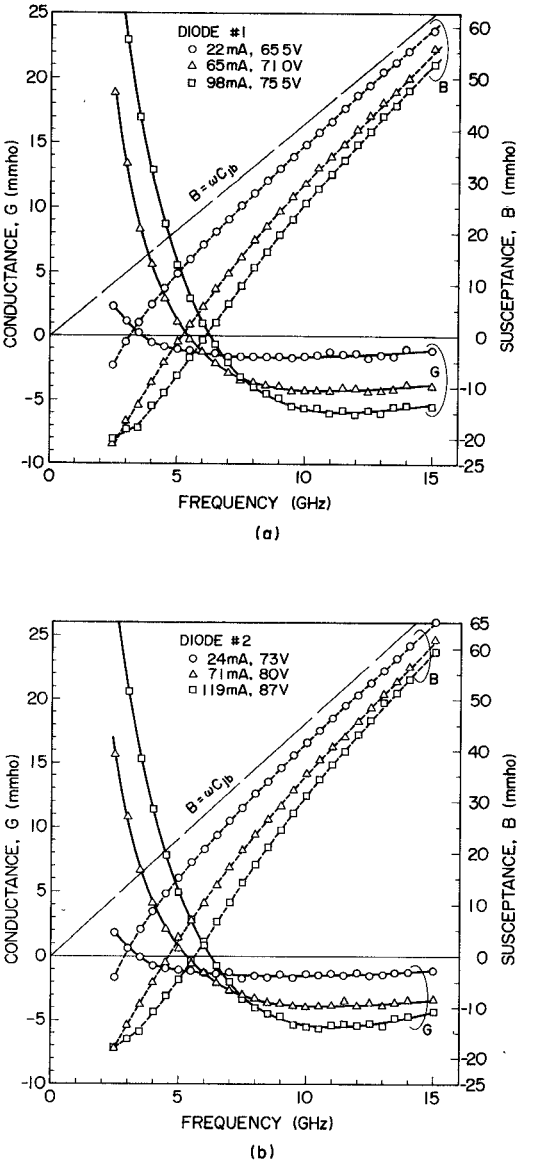

Fig. 7. Example of measured junction admittance. (a) Diode number 1. (b) Diode number 2.

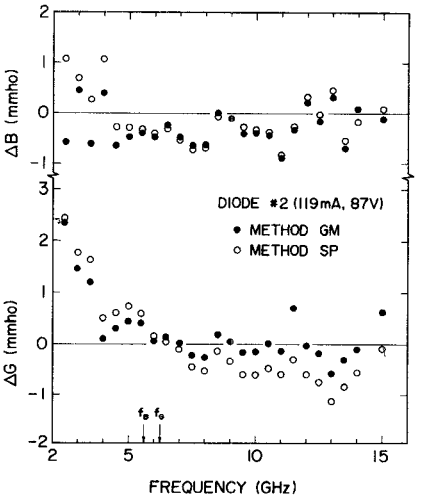

Fig. 8. Comparison of $G + jB$ measured with the present method and methods GM or SP, where $\Delta G = G$ (present method) $- G$ (method GM or SP) and $\Delta B = B$ (present method) $- B$ (method GM or SP).

TABLE II
EXAMPLE OF ESTIMATED SERIES RESISTANCE VARIATION ABOVE BREAKDOWN

	Just Above Breakdown	Above Breakdown
Bias voltage (volt)	70	87
Bias current (mA)	0.2	119
T_j (°C)	30	225
C_j (pF)	0.73	0.67
R_s (ohm)	0.53	0.61*

* $R_s \approx \sqrt{2}R_{si}$, $R_{si} = 0.43\ \Omega$.

TABLE III
CORRECTION TO BE ADDED TO $G + jB$ (DIODE NUMBER 2)

	10 GHz	12.5 GHz	15 GHz
$G_t - G$ (mmho)	-0.07	-0.17	-0.27
$B_t - B$ (mmho)	-0.02	-0.04	-0.04

Note: Bias current equals 119 mA, $\Delta R_s = 0.08\ \Omega$.

factor 2 for a variation of T_j from 25 to 200°C ([17, Fig. 20]). Hence, resultant difference $\Delta R_s \equiv R_s(V) - R_s(V_{br})$ will generally be small, as illustrated in Table II, where C_j above breakdown is the extrapolated value to be mentioned later. Extrapolating the curve in Fig. 6 to a point of this reduced C_j, where the junction seems nearly punched through (see Fig. 11), we have $R_s = R_{si}$ that is roughly equal to the skin resistance of the n^+ and p^+ layer at room temperature. Since the skin resistance is proportional to (resistivity)$^{1/2}$, we obtain $R_s \approx \sqrt{2}R_{si}$ and $\Delta R_s \approx 0.08\ \Omega$ at the elevated T_j. Then the corrections to G and B, calculated from (7) and (8), are seen to be small, as illustrated in Table III.

IV. DISCUSSIONS

The observed phenomenon of $f_B < f_G$ in the present diodes is inconsistent with Misawa's numerical analysis [9], in which, however, the saturation current was assumed to be negligibly small. Meanwhile, Decker *et al.* [18] observed such phenomenon in some of Ge n^+-p-p^+ diodes, and found that it was in conjunction with the decrease of negative-conductance magnitude caused by an excess saturation current due to an injecting contact. Schroeder and Haddad [19] have discussed other possible sources of excess saturation current emerging above breakdown.

Bearing these in mind and assuming a presence of saturation current *a priori*, the following discussions aim mainly at estimating the degree of saturation-current effect in the present diodes, by numerical comparisons with a nonquasistatic analytical theory by Hulin *et al.* [8]. Neglect of carrier diffusion in the theory does not seem to introduce significant errors in the case of Si p^+-n-n^+ diodes [20], [19]. Dependence of measured avalanche frequency upon dc current is also discussed.

A. Saturation-Current Effect

The effect of saturation current is first discussed briefly based upon the expression for active admittance $G + jB$ derived from the theory. $G + jB$ can be rewritten from active impedance Z[4] in [8], after somewhat lengthy manipulations, as

$$G = -\omega C_j \frac{g_1 B_0(1 - B_0) - Q_a^{-1}B_0(1 - g_2)}{(1 - g_2B_0)^2 + (g_1B_0 + Q_a^{-1})^2} \tag{9}$$

$$B = \omega C_j \frac{(1 - g_2B_0)(1 - B_0) + Q_a^{-1}g_1B_0 + Q_a^{-2}}{(1 - g_2B_0)^2 + (g_1B_0 + Q_a^{-1})^2} \tag{10}$$

where

$$B_0 \equiv \omega_a^2/\omega^2$$

$$\omega_a^2 \equiv (2\pi f_a)^2 = 1/L_aC_a = 3\bar{\alpha}'\bar{v}I_{dc}/\epsilon A \tag{11}$$

$$1/Q_a \equiv R_{I_s}/\omega L_a - \omega L_aG_a = 1/\omega\bar{M}\tau_1 - \omega\tau_1\gamma_{Si}/5 \tag{12}$$

$$\tau_1 \equiv l_a/3\bar{v}$$

$$g_1 \equiv \sum_{i=n,p} \frac{\cos\theta_i - \cos(\theta_i + \theta_{di})}{\theta_{di}} \cdot \frac{l_i}{l}$$

$$g_2 \equiv 1 - \frac{l_a}{l} - \sum_{i=n,p} \frac{\sin(\theta_i + \theta_{di}) - \sin\theta_i}{\theta_{di}} \cdot \frac{l_i}{l}.$$

In the preceding equations, L_a, C_a, $\bar{\alpha}'$, $\bar{v}$, R_{I_s}, G_a, $\bar{M}$, and γ_{Si} ($=1.24$ for Si) are those given in [8], and $\omega L_aG_a \ll 1$ is assumed here; f_a equals avalanche frequency; the subscript $i = n$ or p refers to electrons or holes, respectively, l,l_a,l_i equal length of the depletion, avalanche, and drift region, respectively; $\theta_{di} = \omega l_i/v_i$ equals transit angle in the drift region; v_i equals saturated drift velocity of electrons ($i = n$) and holes ($i = p$); and θ_i equals the phase delay given by [8, eq. (7)]. The saturation current affects G and B through Q_a. Note that if $\theta_i = 0$ and $G_a = 0$, (9) and (10) are equivalent to [21, eq. (106)].

Computer simulations of dc current distributions in the present diodes ($N_s = 1 \times 10^{20}$ cm^{-3}, $x_j = 2$ μm, $N_D - N_A = 8 \times 10^{15}$ cm^{-3}) indicate

$$l_a/l \doteqdot 0.35 \qquad l_n/l \doteqdot 0.55 \qquad l_p/l \doteqdot 0.1 \tag{13}$$

where l_a is defined as the length of the region where 90 percent of the current multiplication takes place [22]. Further, α/β (the ratio between electron and hole ionization rates) = 10 will be assumed here for computing θ_i. Taking $\bar{v} = v_n = v_p = 1 \times 10^7$ cm/s and $l = 3.4$ μm, for example, we find that $g_1 = 0.204$, $g_2 = 0.046$ at 6 GHz, and $g_1 = 0.364$, $g_2 = 0.171$ at 12 GHz, where θ_n and θ_p were found to have little effect on g_1 and g_2.

If we assume $|f_G - f_a|/f_a$, $|f_B - f_a|/f_a$, and $|Q_a^{-1}| \ll 1$, we have

$$(f_G - f_B)/f_a = Q_a^{-1}[(1 - g_2)/2g_1 + g_1/(1 - g_2)] \tag{14}$$

[4] G_a in [8, eq. (8)], which seems a typographical error, was corrected into $-G_a$.

$$(f_G - f_a)/(f_B - f_a) = -(1 - g_2)^2/g_1^2$$

from (9) and (10), where Q_a, g_1, and g_2 are the values at f_a. Since g_1, $1 - g_2 > 0$, and $1 - g_2 \gg g_1$ usually hold for $\theta_{dn} \lesssim 1$ rad or $f \lesssim 7$ GHz, we obtain $|f_B - f_a| \ll |f_G - f_a|$ and $f_B \lesssim f_a \lesssim f_G$ according to $Q_a \gtrless 0$. Hence, it is usually allowed to take $f_B = f_a$ without marked error in the present diodes. If desired, Q_a and $\bar{M}$ can be estimated from measured f_B and f_G using (14) and (12). According to [8, eq. (5)], we have

$$\bar{M} \approx 0.26 I_{dc}/(I_{ns} + 0.1 I_{ps}) \quad (15)$$

in the present Si diodes, where I_{ns} and I_{ps} equal electron and hole saturation currents.

B. Dependence of Avalanche Frequency on DC Current

Fig. 9 shows f_a^2 versus dc current density I_d for the investigated diodes, where f_a was taken equal to f_B, as mentioned previously. The values of f_B above 2.5 GHz were obtained by interpolating the susceptance data, while those below 2.5 GHz were evaluated from least squares curve fitting of the measured susceptance by the expression

$$B = \omega C_j(1 - B_0) = \omega C_j - \omega_a^2 C_j/\omega \text{ or } \omega B = C_j(\omega^2 - \omega_a^2) \quad (16)$$

over 2.5–12 GHz. The standard deviation for each fit was found to be less than 0.2 mmho. Equation (16) is a good approximation for (10) with little error (<1 percent) over 2.5–12 GHz, if $f_a \lesssim 2.5$ GHz and $|Q_a| \gtrsim 20$.

Fig. 9 reveals that f_a^2 is sublinear with respect to I_d, contrary to the theoretically well-known relation such as (11). The sublinearity is too large to be ascribed to a possible offset error in f_B mentioned in Section III-B, since the ratio between the measured and true f_B^2 is equal to $1 - 2(C_B + \Delta C)/(\partial B/\partial\omega)_{f_B}$, which is close to 1 and almost frequency independent. Considering that $\bar{\alpha}'$, $\bar{v}$, and ϵ are generally temperature dependent, the discrepancy may be attributed primarily to an increase of junction temperature with I_d. It is then of interest to plot f_a^2/I_d against T_j as shown in Fig. 10. The plots for both diodes are seen to be closely fitted by solid curves calculated with an experimental formula:

$$(f_a^2/I_d)_{T_j} = (f_a^2/I_d)_{30°C}[1 - 1.7 \times 10^{-3}(T_j - 30) + 1.4 \times 10^{-6}(T_j - 30)^2] \quad (17)$$

where $(f_a^2/I_d)_{30°C} = 0.095$ and 0.087 GHz²·cm²/A for diodes numbers 1 and 2, respectively. From (11), we have a field derivative of the average ionization rate $\bar{\alpha}' = 0.129$ (diode number 1) and 0.118 V^{-1} (diode number 2) at $T_j = 30°C$ by taking $\bar{v} = 1 \times 10^7$ cm/s.

The value of $(f_a^2/I_d)_{200°C}/(f_a^2/I_d)_{30°C}$ obtained from (17) agrees well with that computed from (11) using the estimated temperature variation of $\bar{v}$, ϵ, and $\bar{\alpha}'$ as shown below, suggesting that the observed sublinearity in f_a^2 against I_d is indeed due to the variation of T_j. Assuming that v_p varies with T_j at the same rate as v_n [23], we obtain $\bar{v}(200°C)/\bar{v}(30°C) = 0.84$. From the temperature coefficient of ϵ ($\doteqdot 78$ ppm/°C), as inferred from the variation of refractive index in Si [24], we have $\epsilon(30°C)/\epsilon(200°C) = 0.99$. In order to allow for nonnegligible electric-field variation within the avalanche region of the actual diodes, the following definition of $\bar{\alpha}'$ other than the one in [8] is employed for calculating $\bar{\alpha}'$:

$$\bar{\alpha}' \equiv (1/3\bar{v}\tau_{1B})[-\partial(1/M)/\partial E_B]$$

which has been obtained by equating (11) with the expression for ω_a^2 in [21], where τ_{1B} and M are the intrinsic response time and multiplication factor at and around the breakdown field E_B, respectively, such as defined in [25]. For an n-type abrupt junction with $N_D - N_A = 8 \times 10^{15}$ cm^{-3}, numerical calculations between the metallurgical junction and the position where 95-percent electron multiplication takes place give $\bar{\alpha}'(30°C) = 0.125$ V^{-1} and $\bar{\alpha}'(200°C) = 0.113$ V^{-1} under pure electron excitation ($\tau_{1B} = \tau_n$, $M = M_n$ [25]), where the temperature dependence of α and β given in [26] was used. Note that $\bar{v}\tau_{1B}$ is independent of $\bar{v}$ if we take $\bar{v} = (v_n + v_p)/2$. Thus we find

$$\frac{\bar{\alpha}'(200°C)v(200°C)\epsilon(30°C)}{\bar{\alpha}'(30°C)v(30°C)\epsilon(200°C)} = 0.75$$

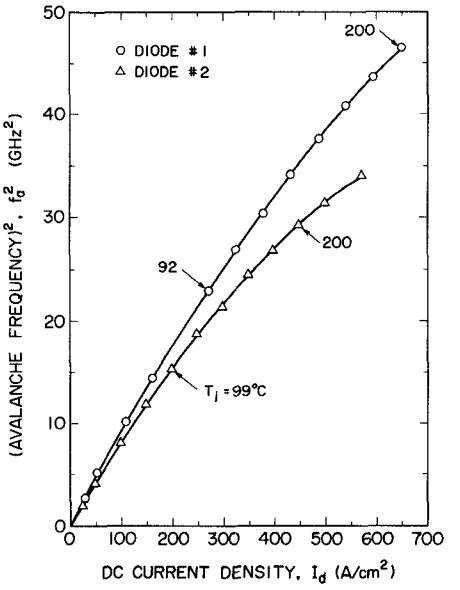

Fig. 9. Dependence of f_a^2 upon dc current density I_d. T_j is estimated junction temperature.

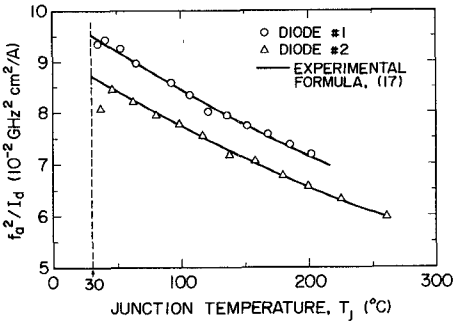

Fig. 10. Plots of f_a^2/I_d against junction temperature.

in agreement with $(f_a^2/I_d)_{200°C}/(f_a^2/I_d)_{30°C} = 0.75$ obtained from (17). It has been also found that, for variation of T_j from 30 to 200°C, l_a/l decreases by only 3 percent and $\bar{\alpha}'(200°C)/\bar{\alpha}'(30°C)$ is nearly independent of $N_D - N_A = 1 \times 10^{16} \sim 5 \times 10^{15}$ cm^{-3}. The details will be reported in the future.

C. Numerical Comparison of Junction Admittance with Theory

Fig. 11 shows the junction capacitance as a function of dc reverse voltage V. The points above breakdown were evaluated by averaging the C_j obtained from (10) with the measured B and calculated g_1, g_2, and Q_a^{-1} over the frequency range $f_a + 1$ GHz $\lesssim f \leq 14$ GHz, where l at breakdown and $\bar{M}$ estimated from measured f_B and f_G were used. They are seen to depend on $\bar{v}$. The lower value of $\bar{v}$ was tentatively employed in order to allow for a possible decrease of $\bar{v}$ and increase of l with increasing T_j. Thus the points for $\bar{v} = 1 \times 10^7$ and 6×10^6 cm/s may be considered the upper and lower bounds for true C_j, respectively. The "true" C_j was then extrapolated within these bounds (dashed line) by smoothly extending the curve for $V \leq V_{br}$. The extrapolated curve gives a useful estimation for l above breakdown.

Fig. 12 shows comparisons between the measured and calculated admittance. In calculating the latter from (9) and (10), l_a, l_n, and l_p were computed from (13) using the extrapolated C_j or l, v_n and v_p in the drift regions were tentatively chosen smaller than $\bar{v}$ in the avalanche region in order to allow for the lower electric field and drift velocity, and $\bar{M}$ was estimated from measured $f_B(=f_a)$ and f_G. It can be seen from Fig. 12 that a good agreement is obtained for both diodes over a wide frequency range if appropriate values are chosen for $\bar{v}$, v_n, and v_p. Especially, at higher dc bias current (②), the set of lower velocities gives a better fit, possibly in accordance with their decrease as T_j increases.

Fig. 13 shows a comparison of $G + jB$ calculated under a realistic value of M(①), negligibly small saturation current (②), and quasistatic approximation with no saturation current (③). Curves ③ are equivalent to those calculated from the Gilden–Hines theory [7]. Comparison of ① and ② reveals that the saturation current shifts B and G towards positive. B is little influenced above f_a, while it undergoes a large modification at lower frequencies. The difference of G between ① and ② is seen to decrease with increasing frequency corresponding to the sign reversal of Q_a from positive to negative at $(1/2\pi)(5/\bar{M}\tau_1^2\gamma_{Si})^{1/2} \doteqdot 9$ GHz. This may explain the fact that both diodes exhibited an oscillation efficiency $\approx$6 percent at 11 GHz (Table I), which is typical of commercial Si p$^+$-n-n$^+$ IMPATT diodes.

From the value of $\bar{M}$ employed for fitting the calculated admittance with the measured one, we can estimate the order of saturation current. Using (15), we find, as a rough estimation, $I_{ns} + 0.1I_{ps} \approx 40$ and 500 μA for curves ① and ② in Fig. 12, which are, however, not consistent with the reverse current $\lesssim$5 nA for $T_j = 25°C$ and $\lesssim$50 μA for $T_j = 200°C$ measured just below breakdown for other diodes belonging to the same lot [27]. The reverse cur-

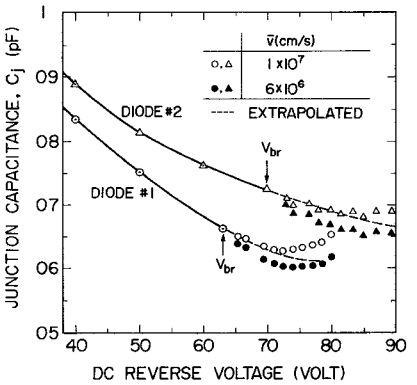

Fig. 11. Junction capacitance versus dc reverse voltage. Dashed line curves represent extrapolated "true" C_j above breakdown.

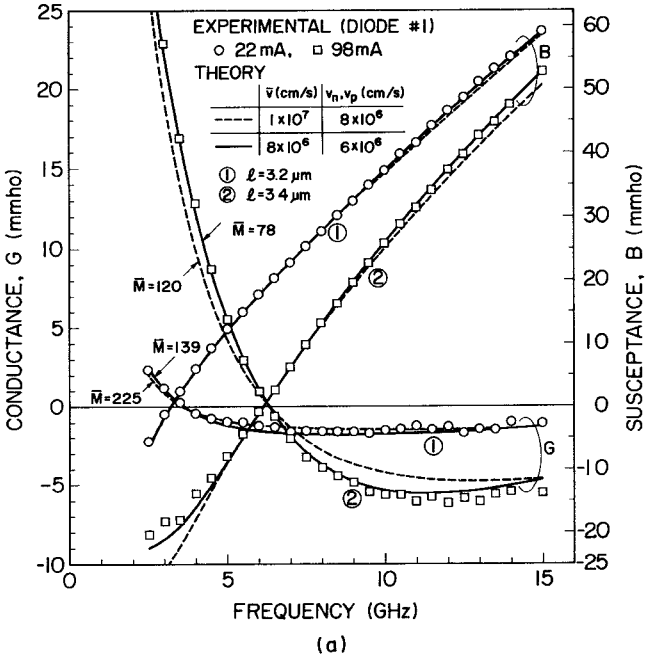

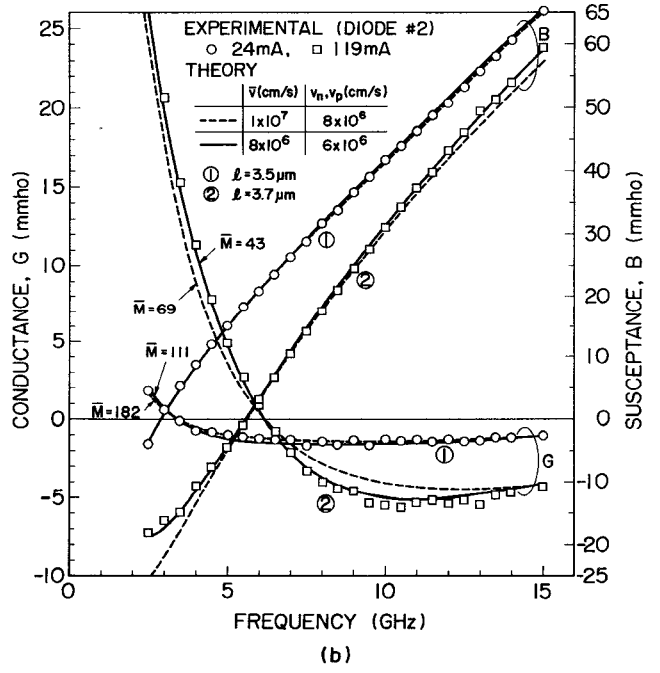

Fig. 12. Numerical comparison of measured junction admittance with theory [8]. (a) Diode number 1. (b) Diode number 2.

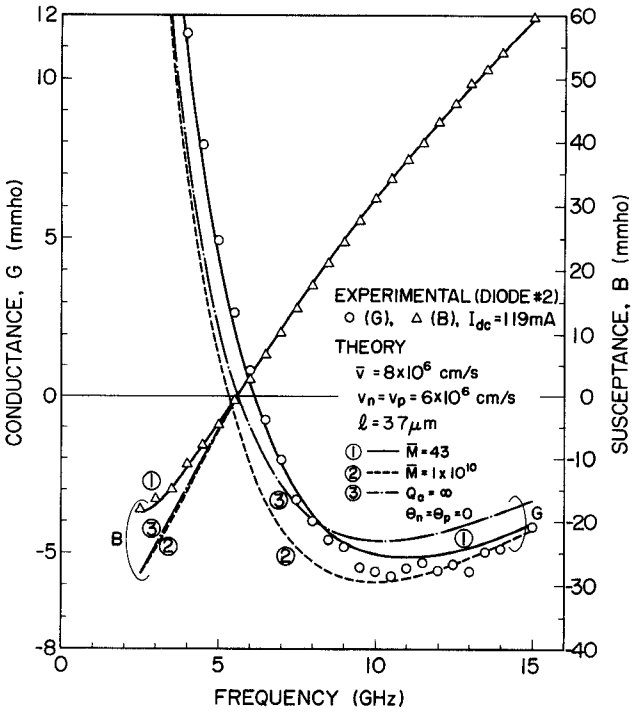

Fig. 13. Comparison between theoretically calculated junction admittances.

rents of the present diodes were measured to be <1 μA on a curve tracer at room temperature. These discrepancies might be accounted for by excess saturation current emerging above breakdown [18], [19].

V. CONCLUSIONS

A method has been developed for broad-band small-signal characterization of an IMPATT diode mounted in a package. With a different combination of known impedances employed in [1]–[3] and a suitable choice of reference planes, this method allows the evaluation of bonding-wire inductance, diode series resistance, and active junction admittance from automatic-network-analyzer measurements. Its applicability is restricted to a case when the package equivalent circuit is represented by Fig. 2, and the metal dummy is a "true" short at T_2 without affecting the coupling-circuit parameters. At higher frequencies of measurement, where the package capacitance C_A is no longer considered as a lumped constant, the present method is still applicable, if the preceding conditions are satisfied.

The measured active admittance has been found to agree well with the theory [8], if a suitable amount of saturation current is postulated. The estimated amount of this current, however, seems larger than the prebreakdown saturation current at corresponding junction temperature. The reason for this is beyond the scope of the present paper. Other possibilities that might have similar effects as the saturation current have not been considered in the present paper. The observed sublinearity of f_a^2 versus dc bias current seems to be due to an increase of junction temperature. This fact, as well as other factors, must be taken into account in designing an IMPATT diode and understanding its temperature dependence.

ACKNOWLEDGMENT

The author wishes to thank S. Okano and E. Murata for valuable discussions and for supplying the diodes.

REFERENCES

[1] C. N. Dunn and J. E. Dalley, "Computer-aided small-signal characterization of IMPATT diodes," *IEEE Trans. Microwave Theory Tech.*, vol. MTT-17, pp. 691–695, Sept. 1969.
[2] D. H. Steinbrecher and D. F. Peterson, "Small-signal model with frequency-independent elements for the avalanche region of microwave negative-resistance diode," *IEEE Trans. Electron Devices*, vol. ED-17, pp. 883–891, Oct. 1970.
[3] J. W. Gewartowski and J. E. Morris, "Active IMPATT diode parameters obtained from computer reduction of experimental data," *IEEE Trans. Microwave Theory Tech.*, vol. MTT-18, pp. 157–161, Mar. 1970.
[4] D. R. Decker, C. N. Dunn, and R. L. Frank, "Large-signal silicon and germanium avalanche diode characteristics," *IEEE Trans. Microwave Theory Tech.* (*Special Issue on Microwave Circuit Aspects of Avalanche-Diode and Transferred Electron Devices*), vol. MTT-18, pp. 872–876, Nov. 1970.
[5] B. B. van Iperen and H. Tjassens, "Measurement of large-signal impedance, optimum ac voltage and efficiency of Si pnn⁺, Ge pnn⁺, and GaAs Schottky barrier diodes," in *Proc. Conf. Microwave and Optical Generation and Amplification* (Amsterdam, The Netherlands), 1970, pp. 7/27–7/32.
[6] ——, "Novel and accurate methods for measuring small-signal and large-signal impedances of IMPATT diodes," *Philips Res. Rep.*, vol. 27, pp. 38–75, 1972.
[7] M. Gilden and M. E. Hines, "Electronic tuning effects in the Read microwave avalanche diode," *IEEE Trans. Electron Devices* (*Special Issue on Semiconductor Bulk-Effect and Transit-Time Devices*), vol. ED-13, pp. 169–175, Jan. 1966.
[8] R. Hulin, M. Classen, and W. Harth, "Circuit representation of avalanche region of IMPATT diodes for different carrier velocities and ionisation rates of electrons and holes," *Electron. Lett.*, vol. 6, pp. 849–850, Dec. 31, 1970.
[9] T. Misawa, "Negative resistance in *p-n* junctions under avalanche breakdown conditions, part II," *IEEE Trans. Electron Devices* (*Special Issue on Semiconductor Bulk-Effect and Transit-Time Devices*), vol. ED-13, pp. 143–151, Jan. 1966.
[10] J. W. Gewartowski, "The effect of series resistance on avalanche diode (IMPATT) oscillator efficiency," *Proc. IEEE* (Lett.), vol. 56, pp. 1139–1140, June 1968.
[11] W. J. Getsinger, "The packaged and mounted diode as a microwave circuit," *IEEE Trans. Microwave Theory Tech.*, vol. MTT-14, pp. 58–69, Feb. 1966.

[12] K. Kurokawa, *An Introduction to the Theory of Microwave Circuits*. New York: Academic, 1969, ch. 1.
[13] A. D. Watt, "VLF radio engineering," in *International Series of Monographs in Electromagnetic Waves*, vol. 14. London, England: Pergamon, 1967, ch. 2.
[14] B. P. Hand, "Developing accuracy specifications for automatic network analyzer systems," *Hewlett-Packard J.*, pp. 16–19, Feb. 1970.
[15] M. Ohtomo, "Small-signal and large-signal impedance measurements of IMPATT diodes with new techniques," presented at the Tech. Group Microwaves, Inst. Elec. Commun. Eng., Japan, MW 73–14, May 1973.
[16] D. Kajfez, "Numerical data processing of reflection coefficient circles," *IEEE Trans. on Microwave Theory Tech.*, vol. MTT-18, pp. 96–100, Feb. 1970.
[17] S. M. Sze, *Physics of Semiconductor Devices*. New York: Wiley-Interscience, 1969, ch. 2.
[18] D. R. Decker, C. N. Dunn, and H. B. Frost, "The effect of injecting contacts on avalanche diode performance," *IEEE Trans. Electron Devices*, vol. ED-18, pp. 141–146, Mar. 1971.
[19] W. E. Schroeder and G. I. Haddad, "Nonlinear properties of IMPATT devices," *Proc. IEEE*, vol. 61, pp. 153–182, Feb. 1973.
[20] R. Hulin and J. J. Goedbloed, "Influence of carrier diffusion on the intrinsic response time of semiconductor avalanches," *Appl. Phys. Lett.*, vol. 21, pp. 69–71, July 15, 1972.
[21] R. L. Kuvås, "Noise in IMPATT diodes: Intrinsic properties," *IEEE Trans. Electron Devices*, vol. ED-19, pp. 220–233, Feb. 1972.
[22] J. J. Goedbloed, "Determination of the intrinsic response time of semiconductor avalanches from microwave measurements," *Solid-State Electron.*, vol. 15, pp. 635–647, 1972.
[23] C. Y. Duh and J. L. Moll, "Temperature dependence of hot electron drift velocity in silicon at high electric field," *Solid-State Electron.*, vol. 11, pp. 917–932, Oct. 1968.
[24] M. Cardona, W. Paul, and H. Brooks, "Dielectric constant measurements in germanium and silicon at radio frequencies as a function of temperature and pressure," in *Solid State Physics in Electronics and Telecommunications*, vol. 1. New York: Academic, 1960, pp. 206–214.
[25] R. L. Kuvås and C. A. Lee, "Quasistatic approximation for semiconductor avalanches," *J. Appl. Phys.*, vol. 41, pp. 1743–1755, Mar. 15, 1970.
[26] C. R. Crowell and S. M. Sze, "Temperature dependence of avalanche multiplication in semiconductors," *Appl. Phys. Lett.*, vol. 9, pp. 242–244, Sept. 15, 1966.
[27] E. Murata, private communication.

Radiation from Curved Dielectric Slabs and Fibers

LEONARD LEWIN, ASSOCIATE MEMBER, IEEE

Abstract—**The form taken by the radiation condition in the local coordinate system, pertinent to the determination by perturbation methods of the radiation from curved radiating structures, is not the same as it is at very great distances. Specifically, it may contain a term that appears as if it were an incoming or growing wave. A detailed analysis is made of the appropriate form of the condition in cylindrical and toroidal systems, and is applied to the calculation of radiation from curved dielectric slabs and fibers.**

I. INTRODUCTION

WITH the introduction of glass fiber as a communication medium, it became necessary to understand and predict the radiation loss or leakage due to bending, with a view both to finding methods of reducing or preventing it, and to determining limits on bending for a given loss.

Marcatili [1] investigated the effects of bending of a dielectric slab in cylindrical coordinates using a method that was basically rigorous, though depending on mathematical asymptotic expansions at a later stage. The same method was applied to obtain an approximation to the leakage from a bent light guide of rectangular cross section. However, this process is not applicable to toroidal coordinates and the curved dielectric fiber.

Manuscript received November 1, 1973; revised February 14, 1974. This study was initiated while the author was on leave at the Department of Electrical and Electronic Engineering, Queen Mary College, London, England, and was supported by an SRC Grant.

The author is with the Department of Electrical Engineering, University of Colorado, Boulder, Colo. 80302.

One method of treating radiation from curved structures is to attempt a perturbation analysis, treating the curvature as a small perturbation to the straight configuration. In so doing one is immediately concerned with matching fields at the structure surface, and hence, with the form of the radiation condition to be applied there. The difficulty arises from the fact that the perturbation analysis presents the field in local coordinate form and the range for which it is valid is limited to dimensions of the order of the size of the structure—in the present case, the bending radius. Since the radiation condition has to be applied at "infinity," i.e., at a distance much greater than the bending radius, the local coordinate form is quite useless. The radiation condition has to be inferred by an indirect process before it can be applied. It needs to be stressed that an "outward-looking" wave in the local coordinates is not necessarily (and in general, is not) the appropriate form to satisfy the radiation condition at very large distances. Thus the outgoing Hankel function $H_\nu^{(2)}(k\rho)$ behaves like an outgoing wave when $k\rho \gg \nu$, but looks more like a sum of a growing and an evanescent wave when $k\rho$ is small. To require only the evanescent term would be erroneous.

Since the cylindrical coordinate solution can, in any case, be set up rigorously, it might be asked what purpose is served by first using it to determine the radiation condition, and then applying this condition to a perturbation analysis. The advantage is threefold. It gives a better insight into what is going on, and may therefore indicate ways of controlling the radiation. Moreover, to get an